Protein Engineering, Design and Selection, 2022, **35**, 1–14
https://doi.org/10.1093/protein/gzab032
Original Article

Modifying pH-sensitive PCSK9/LDLR interactions as a strategy to enhance hepatic cell uptake of low-density lipoprotein cholesterol (LDL-C)

Lital Ben-Naim[1], Isam Khalaila[1,*] and Niv Papo[1,2,*]

[1]Avram and Stella Goldstein-Goren Department of Biotechnology Engineering, Faculty of Engineering, Ben-Gurion University of the Negev, Beer-Sheva 84105, Israel
[2]The National Institute for Biotechnology in the Negev, Ben-Gurion University of the Negev, Beer-Sheva 84105, Israel
*To whom correspondence should be addressed. E-mail: papo@bgu.ac.il (Niv Papo); isam@bgu.ac.il (Isam Khalaila)

Abstract

LDL-receptor (LDLR)-mediated uptake of LDL-C into hepatocytes is impaired by lysosomal degradation of LDLR, which is promoted by proprotein convertase subtilisin/kexin type 9 (PCSK9). Cell surface binding of PCSK9 to LDLR produces a complex that translocates to an endosome, where the acidic pH strengthens the binding affinity of PCSK9 to LDLR, preventing LDLR recycling to the cell membrane. We present a new approach to inhibit PCSK9-mediated LDLR degradation, namely, targeting the PCSK9/LDLR interface with a PCSK9-antagonist, designated Flag-PCSK9$_{PH}$, which prevents access of WT PCSK9 to LDLR. In HepG2 cells, Flag-PCSK9$_{PH}$, a truncated version (residues 53–451) of human WT PCSK9, strongly bound LDLR at the neutral pH of the cell surface but dissociated from it in the endosome (acidic pH), allowing LDLR to exit the lysosomes intact and recycle to the cell membrane. Flag-PCSK9$_{PH}$ thus significantly enhanced cell-surface LDLR levels and the ability of LDLR to take up extracellular LDL-C.

Graphical Abstract

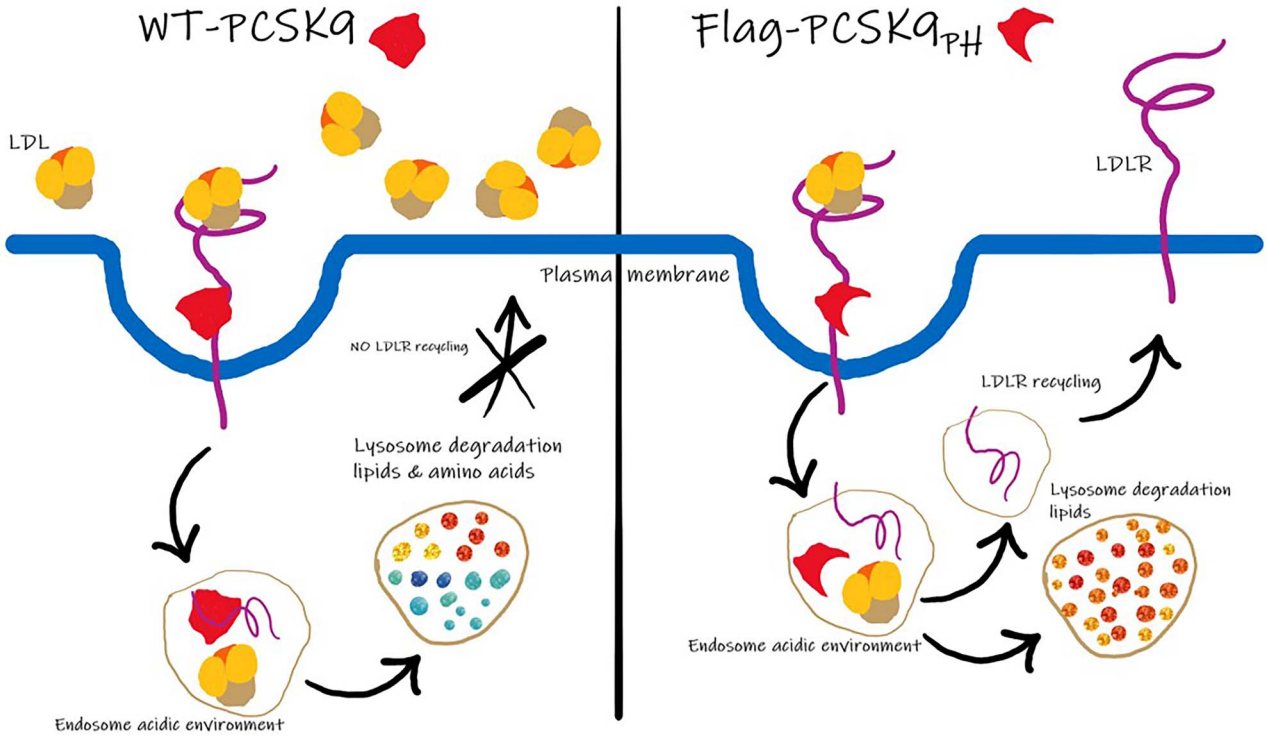

Keywords: antagonist, cardiovascular disease, LDL-receptor, low-density lipoprotein cholesterol, proprotein convertase subtilisin/kexin type 9, protein engineering

Received: June 14, 2021. **Revised:** November 29, 2021. **Editorial decision:** December 8, 2021. **Accepted:** December 8, 2021

Introduction

It is currently held that a major risk factor for most cardiovascular diseases (CVDs) is a high blood level of cholesterol, which may lead, in some cases, to the build-up of cholesterol-containing plaque along the walls of the large arteries (Hansson and Hermansson 2011; Libby 2002) and hence to the narrowing (Bui *et al.* 2009; Cleeman 2001; Moore *et al.* 2013) and blockage of those arteries. A reduction of high blood cholesterol levels may thus contribute to a decrease in CVD morbidity and mortality (Virani *et al.* 2020). However, current therapies with statins [inhibit the biosynthesis of cholesterol (Stancu and Sima 2001)] and/or ezetimibe [inhibits absorption of intestinal cholesterol (Cannon *et al.* 2015; Mancini *et al.* 2011)] for lowering levels of circulating low-density lipoprotein cholesterol (LDL-C) are not always effective (Attie and Seidah 2005; Dubuc *et al.* 2004) and may be associated with drug intolerance (Reiner 2014) or a range of side effects—some severe (e.g. Stolk *et al.* 2006) and others less so (Reiner 2014; Sirtori 2014).

In attempts to develop new drugs, some protein engineering studies are currently focusing on proprotein convertase subtilisin/kexin type 9 (PCSK9) (Matta *et al.* 2020; Schulz *et al.* 2015) as a potential drug target. To understand the rationale underlying this drug development—and that of the current study—it is necessary to first take a very brief look at the structures of LDL-C and PCSK9 and the mechanism of their interaction in the human body. LDL-C is composed of cholesteryl esters (~65% of plasma cholesterol) (Segrest *et al.* 2001), triglycerides and phospholipids (enabling transportation through the blood), and apolipoprotein B-100 (apoB), which is anchored to the surface of the phospholipid layer. PCSK9 is synthesized in a number of organs and tissues in the human body (O'Connell and Lohoff 2020; Stoekenbroek *et al.* 2018), including the liver. The proenzyme form of PCSK9 that is produced in hepatocytes is a serine endoprotease consisting of four domains: a signal peptide (resides 1–30), a prodomain (residues 31–152), a catalytic domain (residues 153–451) and a C-terminal cysteine- and histidine-rich domain (residues 452–692) (Horton *et al.* 2009). The signal peptide is cleaved off the molecule in the endoplasmic reticulum (ER), and the zymogen proPCSK9 (residues 31–692, Mw ~74 kDa) then undergoes a single autocatalytic cleavage reaction between the prodomain and catalytic domain, allowing PCSK9 to exit into the circulation as a mature and functional protein (Benjannet *et al.* 2004). In the mature protein, the prodomain (~14 kDa) remains noncovalently attached to the catalytic domain (~60 kDa), with the former acting as a chaperone to assist in the folding of the matured PCSK9 protein and to prevent it from acting as a serine protease by physically blocking a key catalytic triad of residues, D186, H226 and S386 (Costet *et al.* 2008; Wierød *et al.* 2016).

In the liver, an interaction takes place, at physiological pH (~7.4), between the low-density lipoprotein receptor (LDLR) protein on the hepatocyte surface and LDL-C, with the LDLR N-terminal ligand-binding domain (LBD; L3-L7 cysteine-rich repeats) binding to its ligand, apoB (Hevonoja *et al.* 2000), in LDL-C (Brown *et al.* 1997). The LDLR–LDL-C complex triggers the formation of a clathrin-coated vesicle that is rapidly internalized into the cell by endocytosis and becomes an early endosome (Lakadamyali *et al.* 2006; McMahon and Boucrot 2011). In the slightly acidic endosome environment (pH ~6), the LDLR–LDL-C complex undergoes dissociation, and LDL-C is delivered to the lysosomes for degradation. The free cholesterol is then metabolized further inside the cell (Go and Mani 2012; Luo *et al.* 2017), and LDLR is recycled back to the cell surface, ready to take up LDL-C particles (Blacklow 2007).

In parallel, a process triggered by PCSK9 for the down-regulation of cell-surface LDLR levels takes place. The process starts with the binding of the PCSK9 catalytic domain to the EGF-A domain of LDLR on the hepatocyte surface (Zhang *et al.* 2007, 2008). The PCSK9–LDLR complex is then internalized via clathrin-mediated endocytosis (Fernández-Higuero *et al.* 2016; Lodish *et al.* 2000; Slater *et al.* 1984) before proceeding to the endosome. The binding affinity of the complex at the acidic pH of the endosome (K_D of 1 nM–8 nM) is two orders of magnitude higher than that at the cell surface (K_D of 170 nM–750 nM, pH 7.4) (Fisher *et al.* 2007; Lambert *et al.* 2012), with the tight binding in the endosome preventing the complex from dissociating (Piper *et al.* 2007) before it is directed to the lysosomes for degradation (Gencer *et al.* 2015; Schulze *et al.* 2009; Xu and Ren 2015). This PCSK9 function (i.e. binding to LDLR and directing it to lysosomal degradation, thereby preventing it from recycling back to the cell membrane) reduces the level of LDLR on the hepatocyte surface, which results in increased levels of LDL-C in the blood (Awan *et al.* 2014; Horton *et al.* 2007; McNutt *et al.* 2007).

A few studies have sought to provide mechanistic explanations for the LDLR–LDL-C and LDLR–PCSK9 interactions. It seems that at neutral pH, LDLR has an 'open' (or extended) conformation, ready to bind LDL-C. In contrast, in the lower pH environment of the early endosome, LDLR undergoes a conformational change to a 'closed' conformation, in which the R4 (residues Cys127 to Cys163) and R5 (Cys176 to Cys210) LBD repeats move inward to interact with the YWTD/β-propeller domain (Ile377 to Gly642) by hydrophobic and charged interactions, thus modulating LDLR conformation as a function of pH (Beglova *et al.* 2004; Rudenko *et al.* 2002). The closed LDLR conformation enables LDL-C to detach from the LDLR–LDL-C complex and LDLR to exit the endosome and recycle back to the cell surface (Beglova and Blacklow 2005; Jeon and Blacklow 2005; Martínez-Oliván *et al.* 2015).

When PCSK9 binds to LDLR, it prevents the formation of the receptor's closed structure. In particular, at the lower pH of the endosome (pH ~6), the positively charged C-terminal (cysteine-histidine-rich domain) of PCSK9 binds strongly to the negatively charged LBD of LDLR (Holla *et al.* 2011a; Tveten *et al.* 2012; Yamamoto *et al.* 2011), thereby 'locking' LDLR and preventing it from adopting the closed conformation needed for its recycling and, instead, directing it to the lysosomes for degradation. Consequently—and importantly for this study—at acidic pH, PCSK9 remains bound to LDLR, and LDLR fails to recycle back to the cell surface (Tveten *et al.* 2012; Zhang *et al.* 2008). Not surprisingly, it was previously observed that PCSK9 lacking the C-terminal domain (needed for its strong binding with the LDLR) did not lead to LDLR degradation (Holla *et al.* 2011a).

With the above background in mind, our strategy for the development of a lead compound was based on manipulating the pH-dependent interaction between PCSK9 and LDLR. To this end, we sought to engineer a PCSK9 antagonist based on a

truncated version (residues 53–451) of the human PCSK9 protein (lacking the N-terminal and C-terminal domains). Among the putative antagonists that we engineered, the most efficient was a truncated protein with a Flag tag on the N-terminal, which we designated Flag-PCSK9$_{PH}$. After high-affinity binding of both recombinant and cell-expressed LDLR to Flag-PCSK9$_{PH}$ [which would thus compete with wild-type (WT) PCSK9] at the neutral pH of the hepatocyte surface, the Flag-PCSK9$_{PH}$/LDLR complex was internalized into the hepatic cell and there, at the acidic pH of the endosome, Flag-PCSK9$_{PH}$ dissociated from LDLR, thereby allowing the LDLR to escape lysosomal degradation and recycle back to the cell membrane. This process, in turn, led to an increase in the number of membranal LDLR molecules available to bind and clear LDL-C particles, to increase LDL-C uptake into cells, and hence to reduce circulating LDL-C levels.

Materials and Methods

Expression and purification of PCSK9 in *Escherichia coli*

To produce the shortest, but still active, version of PCSK9, proteins of two different lengths were constructed, with one containing the sequence of human PCSK9 spanning residues Ala53-Lys421 and the other, the Ala53-Ala451 sequence. Both contained the prodomain and catalytic domain, but lacked the C-terminal domain, and both were based on the human PCSK9 NCBI Reference Sequence: NP_777596.2. The Ala53-Lys421 and Ala53-Ala451 sequences were polymerase chain reaction (PCR) amplified from the pcDNA3-PCSK9-WT plasmid (kindly provided by the laboratory of Thomas Legace, University of Ottawa Heart Institute, Ottawa, Canada), using the primers listed in Table , and inserted into the pET24b-His plasmid (EMBL Heidelberg, Germany) between the NdeI and XhoI sites (New England BioLabs, MA, USA). The resulting PCSK9(53-421)-His, PCSK9(53-451)-His, His-PCSK9(53-451)-His proteins were produced in *E. coli* BL21 cells, as previously described (Salowe *et al.* 2016), where PCSK9(53-451)-His and His-PCSK9(53-451)-His are henceforth designated PCSK9$_{PH}$-His and His-PCSK9$_{PH}$-His, respectively. After an overnight incubation, the cells were pelleted by centrifugation at 4500 *g* for 15 min. One gram of cell pellets was suspended and sonicated in 4 ml of lysis buffer (50 mM Hepes pH 8, 200 mM NaCl, 5% glycerol, 0.1 mM $CaCl_2$, 0.1 mM CHAPS) supplemented with Protease Inhibitor Cocktail (A_2S technologies, Yavne, Israel), treated with DNase I (New England BioLabs) for 30 min on ice, and centrifuged at 20 000 *g* for 30 min at 4°C. After removal of the cell debris, the supernatant was filtered through a 0.22-μm Stericup (Millipore, Burlington, MA, USA), loaded on a 5-ml Ni-NTA affinity column (GE Healthcare, NJ, USA) equilibrated with 50 mM Hepes (pH 8.0), 200 mM NaCl, 5% glycerol and 0.1 mM $CaCl_2$, and washed with 20 ml of equilibration buffer plus 50 mM imidazole. Proteins were eluted with equilibration buffer complemented with 400 mM imidazole and subjected to further purification by size-exclusion chromatography (SEC) using a Superdex-75 16/600 column (GE Healthcare) equilibrated in equilibration buffer with 0.05% n-octyl-β-glucoside instead of imidazole. The yield of each purified protein was determined using a DS-11 microvolume spectrophotometer (Denovix, DE, USA), and purity was confirmed by SDS-PAGE with Coomassie Brilliant Blue (Bio-rad, CA, USA) staining. To verify the identity of the proteins by mass spectrometry, excised SDS-PAGE gel bands were denatured, reduced, alkylated and digested with trypsin, and the digested peptides were then subjected to tandem mass spectrometry (MS/MS) analysis on a LTQ-Orbitrap XL ETD instrument, as described previously (Roth *et al.* 2013) [Ilse Katz Institute for Nanoscale Science and Technology Shared Resource Facility, Ben-Gurion University of the Negev (BGU)].

Expression and purification of PCSK9 in a mammalian system

The full-length sequence encoding PCSK9 (NCBI Reference Sequence: NM_174936.4), representing residues Gln30–Gln692, was amplified and subcloned into the pCDNA3.1 mammalian expression plasmid (a generous gift from Ran Taube, BGU). The construct was designed to include a C-terminal 6 × His-tag (designated His-tag), and the secretion signal peptide honeybee melittin replaced the native PCSK9 signal peptide, as described previously (Hampton *et al.* 2007). The sequence encoding PCSK9 Ala53–Ala451 was also amplified by PCR and inserted into the pCDNA3.1 plasmid between the XhoI and NotI sites (New England BioLabs), fused to an N-terminal His-tag or a FLAG (DYKDDDDK) tag (Table). In addition, to prevent cleavage and inactivation of PCSK9 by furin, a protease expressed in mammalian cells (Lambert *et al.* 2009), a point mutation of R281S was incorporated into all pcDNA3.1 constructs, as described previously (Edelheit *et al.* 2009). The proteins His-PCSK9$_{PH}$ and Flag-PCSK9$_{PH}$ were expressed in the FreeStyle™ 293-F mammalian expression system (Invitrogen, CA, USA), as follows. Cells in suspension (1 L) were transfected with pcDNA3.1-PCSK9-His, pcDNA3.1-His-PCSK9$_{PH}$ or pcDNA3.1-Flag-PCSK9$_{PH}$, according to the manufacturer's protocol. Four days after transfection, cultures were harvested by centrifugation at 1200 rpm for 20 min. The supernatant obtained for full-length WT PCSK9 or His-PCSK9$_{PH}$ was loaded onto 2 ml of Ni-NTA Sepharose beads (Invitrogen) in a gravity flow column, equilibrated with 50 mM Tris–HCl, pH 7.4, 300 mM NaCl, 1 mM $CaCl_2$, and 2 mM β-mercaptoethanol, and washed with 20 ml of equilibration buffer plus 20 mM imidazole. Bound PCSK9 proteins were eluted in 10 ml of equilibration buffer supplemented with 350 mM imidazole, followed by dialysis against phosphate-buffered saline (PBS) and concentration using a Vivaspin with a cutoff of 5 kDa (Vivaproducts, MA, USA). The supernatant obtained for Flag-PCSK9$_{PH}$ was loaded onto anti-DYKDDDDK G1 affinity resin (GenScript, NJ, USA) in a gravity flow column. All steps were performed according to the manufacturer's protocols. The Flag-PCSK9$_{PH}$ protein was eluted with 50 mM Tris–HCl and 150 mM NaCl, pH 7.4. The yield of each purified protein (WT PCSK9, His-PCSK9$_{PH}$ and Flag-PCSK9$_{PH}$) was determined using a DS-11 microvolume spectrophotometer (Denovix), and purity was confirmed by SDS-PAGE gel stained with Coomassie Brilliant Blue (Bio-Rad).

Cell culture

HepG2 adherent cells (ATCC, VA, USA), which endogenously express LDLR, were cultured at 37°C under a 5% CO_2 atmosphere in a complete growth medium composed of DMEM, High Glucose with stable Glutamine (Biological Industries,

Beit Haemek, Israel), supplemented with 10% fetal bovine serum (FBS), 100 U/ml penicillin and 100 μg/ml streptomycin.

Analysis of cell-surface LDLR by flow cytometry

For the detection of cell-surface LDLR expression, HepG2 cells were seeded into a 96-well plate (4×10^4/well) and cultured in the complete growth medium. After 48 h, cells were harvested using Non-enzymatic Cell Dissociation Solution (Biological Industries), washed twice with a wash buffer of PBSA [PBS supplemented with 1% bovine serum albumin (BSA)], and centrifuged for 5 min at 200 *g*. Cells were then incubated with phycoerythrin (PE)-conjugated mouse antihuman LDLR antibody (1:20 dilution in Wash Buffer; R&D Systems, MN, USA) at 4°C for 1 h, followed by three cycles of washing and centrifugation for 5 min at 250 *g*. Cells were resuspended in 200 μl of PBS, and PE fluorescence was quantified with an Accuri C6 Flow Cytometer (BD Biosciences, CA, USA). Unstained cells were used to determine the background signal. For upregulation of LDLR expression, HepG2 cells were cultured in complete medium and after 24 h were treated in one of two ways: (i) with medium containing 10 μM pravastatin (Sigma–Aldrich, Rehovot, Israel) for 12, 24, or 48 h or 4 days, or (ii) with complete culture medium supplemented with 5% lipoprotein-deficient serum (LPDS) (ADI-Alpha Diagnostic, TX, USA) instead of FBS, for 24 h, according to the manufacturer's protocol.

Analysis of truncated PCSK9 binding to cell-expressed LDLR by flow cytometry

HepG2 cells were treated with a medium containing 5% LPDS and were harvested after 24 h using Cell Dissociation Solution (Biological Industries), as mentioned above. After washing and centrifugation, cells were incubated with 1 μM $PCSK9_{PH}$-His at 4°C for 1 h, with agitation, in binding buffer (25 mM Hepes pH 7.4, 150 mM NaCl, 1 mM $CaCl_2$, 0.005% Tween). Cells were washed with PBSA and then incubated with rabbit antihuman PCSK9 antibody (1:50 dilution in Wash Buffer; Novus Biologicals, Ontario, Canada) for 1 h at 4°C, followed by a secondary antirabbit-PE antibody for 30 min at 4°C. After three cycles of washes, cells were resuspended in 200 μl of PBS and analyzed with an Accuri C6 Flow Cytometer. A control sample of cells was incubated with a secondary antirabbit-PE antibody to determine the fluorescence background signal. The data were analyzed using FlowJo (Tree Star Inc., OR, USA) analysis software.

Localization of PCSK9 proteins, LDLR and lysosomes by immunofluorescence

$PCSK9_{PH}$-His was labeled with Alexa Fluor 647 (Invitrogen) at a 1:3 (protein:dye) molar ratio according to the manufacturer's protocol. The labeled protein (0.5 mg/ml) was buffer-exchanged into PBS overnight at 4°C, using GeBAflex-Midi Dialysis Tubes, 3.5-kDa cutoff (Gene Bio-Application, Yavne, Israel). HepG2 cells (without upregulation of LDLR expression) were transfected with a fluorescently labeled LDLR plasmid by using pcDNA4-LDLR-EYFP (kindly provided by the laboratory of Trond Paul Leren, Oslo University Hospital, Norway) and the Lipofectamine® 3000 transfection reagent (Thermo Fisher Scientific, MA, USA), according to the product protocol. Forty-eight hours after transfection, 3×10^4 cells were subcultured in μ-slide 8-well microscopy chambers (ibidi, Martinsried, Germany) in 200 μl of complete medium and incubated for additional 24 h in a humidified incubator at 37°C and 5% CO_2. Cells were washed with PBS, treated with 1 μM of the Alexa Fluor 647-labeled $PCSK9_{PH}$-His, and incubated for 10 min or 1.5 h in fresh complete medium prior to imaging. To label cellular nuclei, Hoechst 33342 (Thermo Fisher Scientific) at a final concentration of 0.1 μg/ml was added to each well.

A similar experiment was performed for Alexa Fluor 647-labeled WT PCSK9-His and Flag-$PCSK9_{PH}$. In this experiment, blue fluorescent protein (BFP) was fused to LDLR cDNA at its C-terminal by PCR amplification and subcloned at NotI/XbaI into pcDNA4-LDLR-EYFP, thereby replacing the EYFP with the BFP sequence. A plasmid coding for a lysosome-associated membrane protein-1 fused to GFP was used to label lysosomes (LAMP1-mGFP, Addgene Cambridge, MA, USA). HepG2 cells were cotransfected with pcDNA4-LDLR-BFP and LAMP1-mGFP plasmids using Lipofectamine 3000, according to the manufacturer's protocol. At 48 h post-transfection, the cells in the μ-slide 8-well plate were incubated for 2 h with either 1 μM labeled WT PCSK9-His or 1 μM labeled Flag-$PCSK9_{PH}$.

Immunofluorescence analyses were performed with a laser-scanning ZEISS LSM-880 confocal microscope (Ilse Katz Institute for Nanoscale Science and Technology Shared Resource Facility, BGU). Confocal Z-series stacks (step size 200 nm) were acquired using the Airyscan detector, a 63× Plan-Apochromat 1.4NA DIC oil immersion objective (Zeiss, Munich, Germany) and the 405 nm (blue fluorescence), 488 nm (green/yellow fluorescence) and 633 nm (far-red fluorescence) laser lines. Zeiss Zen 2.3 (black edition) software was used to control the microscope, to adjust the spectral detection for the emission of Hoechst (or BFP), enhanced yellow fluorescent protein (EYFP)/GFP and Alexa Fluor 647 fluorochromes, and to process the Airyscan raw images.

Binding affinity measurements of purified PCSK9 and LDLR by SPR

The binding affinity of purified PCSK9 to purified LDLR was determined by using surface plasmon resonance (SPR) spectroscopy on a ProteOn XPR36 instrument (Bio-Rad) at 25°C. The recombinant human LDLR extracellular region (Ala22-Arg788) (BioLegend, CA, USA), 0.6 μg or 1.2 μg, was immobilized on the ProteOn GLC sensor chip with the amine coupling reagents 1-ethyl-3-(3-dimethylaminopropyl)carbodiimide hydrochloride (EDAC) and N-hydroxysulfosuccinimide (sulfo-NHS) (ProteOn amine coupling kit), according to the manufacturer's instructions (Xpr *et al.* 2005). BSA, 3 μg, was immobilized on the chip and used as a control for nonspecific protein binding. Purified WT PCSK9 or a truncated PCSK9 protein (WT-PCSK9-His, His-$PCSK9_{PH}$-His, $PCSK9_{PH}$-His, His-$PCSK9_{PH}$ or Flag-$PCSK9_{PH}$) served as the analyte, which was applied over the chip in five concentrations (for each protein the concentrations lay in the range 0 nM–20 nM, 0 nM–250 nM or 0 nM–500 nM) at a flow rate of 30 μl/min, with a binding buffer at physiological pH 7.4 or acidic pH 5.5 [containing 150 mM NaCl, 1 mM $CaCl_2$, 0.005% (v/v) Tween-20, plus either 25 mM Hepes (pH 7.4) or 25 mM sodium acetate (pH 5.5)], giving a neutral or acidic environment for the binding reactions, respectively. As the positive control, a commercial recombinant human PCSK9-His (Novoprotein,

Shanghai, China) was used. The association between LDLR and the PCSK9 protein was measured as each PCSK9 protein was allowed to flow over the surface-immobilized ligand (i.e. LDLR), and the dissociation was measured during continuous flow of the binding buffer for 10–20 min. For studies of LDLR (as the analyte) binding to His-PCSK9$_{PH}$ (as the ligand), the purified His-PCSK9$_{PH}$ was immobilized via its His-tag onto an HTG Sensor Chip (Bio-Rad), according to the manufacturer's instructions. For each protein–ligand complex, binding sensorgrams were generated. To obtain the dissociation constants (K_D) for the interaction of each PCSK9 protein (analyte) with LDLR (chip-immobilized ligand), iterations of the kinetic parameters of the association rate constant (k_{on}) and dissociation rate constant (k_{off}) were used to build 'predicted' sensorgrams and to calculate an Rmax (maximal response) value. For each set of 'predicted' versus observed sensorgrams, a chi^2 value was then calculated (chi^2 = (obs − pred)^2/(n − p), where n is the number of measured points in the observed sensorgram and p is the statistical model's degrees of freedom). A statistical chi^2 value was considered valid if its value was <10% of the value of Rmax. Since the affinity constant $K_D = k_{off}/k_{on}$, the calculated k_{off} and k_{on} were then used to determine K_D. An alternative approach that was also used was based on steady-state analysis, in which K_D was obtained from a plot of the equilibrium binding responses (R_{eq}) against different concentrations of the analyte (i.e. PCSK9 proteins). The Proteon software includes a steady-state affinity model that allows calculation of binding affinity from such a plot, as described previously (Surdo *et al.* 2011). Here again, a result was considered valid only if the calculated chi^2 value was <10% of the Rmax.

Analysis of cell-surface LDLR display levels upon treatment with PCSK9 proteins

HepG2 cells were seeded in a 24-well plate at 3 × 10^4 cells/well and allowed to attach and grow in complete growth medium overnight in a humidified incubator at 37°C and 5% CO_2. On the following day, cells were washed with PBS and maintained in a culture medium supplemented with 5% LPDS for 24 h to increase LDLR levels on the cell surface. On the third day, cells were suspended in PBS and treated with 1 μM WT PCSK9-His, 1 μM Flag-PCSK9$_{PH}$ or a combination of 1 μM WT PCSK9-His and 1 μM Flag-PCSK9$_{PH}$ and incubated for 12 h in a 37°C incubator. Cells were then detached using Cell Dissociation Solution (nonenzymatic) (Biological Industries), washed with PBSA buffer, and centrifuged for 5 min at 250 *g*. Cells were incubated with PE-conjugated mouse antihuman LDLR antibody (1:20 dilution in PBSA; R&D Systems) at 4°C for 1 h, followed by three washing cycles. Cells were resuspended in 200 μl of PBS, and cell-surface LDLR was detected by quantification of PE fluorescence with an Accuri C6 flow-cytometer analyzer (BD Biosciences).

Fluorescent LDL-C cell uptake

HepG2 cells were cultured as described above for 2 days, and on the third day the cells were treated in one of four ways, namely, with 4 μM WT-PCSK9, 4 μM Flag-PCSK9$_{PH}$, 4 μM WT-PCSK9 plus Flag-PCSK9$_{PH}$, or PBS (as a vehicle), and incubated for 12 h in a 37°C incubator. At the end of the treatment, the culture medium was replaced with 20 μg/ml LDL-DyLight™ 550 (Cayman Chemical Company, MI, USA) diluted in serum-free culture medium (1:100). After incubation for 6 h at 37°C, excess LDL-Dylight 550 was removed by three PBS washes, and cells were detached using trypsin (Biological Industries) and centrifuged at 250 *g* for 5 min. Harvested cells were filtered through a 35-μm cell strainer tube (Corning, NY, USA). LDL-Dylight 550 uptake was measured using flow cytometry analysis on a Synergy SY3200 Cell sorter (Sony Biotechnology, CA, USA) (NIBN Cytometry, Affinity and Imaging Unit, BGU) with a filter capable of measuring excitation and emission wavelengths of 540 nm and 570 nm, respectively. LDL uptake was determined as the mean total intensity of intracellular DyLight 550 fluorescence signal of 10 000 events/well for each treatment condition. Experiments were performed in duplicate and repeated three times. For statistical analysis, data are reported as means ± standard deviation (SD). Significant differences between groups were evaluated by an unpaired Student's t-test, where $P < 0.0001$ was considered statistically significant. Graphs were created using GraphPad 6 software (GraphPad, CA, USA).

Thereafter, to visualize LDL-C uptake, HepG2 cells were subjected to high-throughput fluorescent confocal microscopy, as follows; cells were plated on 96-well optical black plates with clear bottoms (Thermo Scientific, MA, USA), at a density of 20 000 cells/well, and cultured with 5% LPDS, as described above. Incubation was continued for 6 h with 100 μl/well of medium containing LDL-DyLight 550. After three cycles of PBS washes, the cell nuclei were stained with Hoechst 33342 at a final concentration of 0.1 μg/ml in a serum-free medium. The plates were viewed through an Operetta microscope (PerkinElmer, MA, USA) with a ×40 wide-angle lens. Images were captured using excitation wavelengths of 405 nm for fluorescent nuclei (blue) and 526 nm for DyLight 550 (yellow). For each well, 23 fields per well were captured, and the data were analyzed using Columbus image analysis software (PerkinElmer). Images were imported into the Fiji version of the image processing software ImageJ. Colocalization analysis was performed with coloc2 and JACop plugins with a measure of the overlapping coefficient values.

Results

Expression and purification of truncated PCSK9 in *E. coli*

As the first step toward realizing our aim of developing a pH-dependent PCSK9 protein antagonist that binds to LDLR with high affinity at physiological pH and dissociates from the receptor at acidic pH, a truncated PCSK9 protein was designed. The recombinant truncated PCSK9 (designated PCSK9$_{PH}$, residues 53–451) was derived from the human WT PCSK9 (residues 31–692) (NCBI Reference Sequence: NP_777596.2) and comprised a short version of the prodomain (residues 53–152) and the catalytic domain (residues 153–451). As mentioned above, the prodomain is required for overall protein folding and for preventing the mature PCSK9 from acting as a serine protease (PCSK9 undergoes autocleavage to convert from a zymogen to an active enzyme), and the catalytic domain is required for the initial binding to the LDLR EGF-A domain. The C-terminal Cys/His-rich domain (residues 452–692) was removed, since

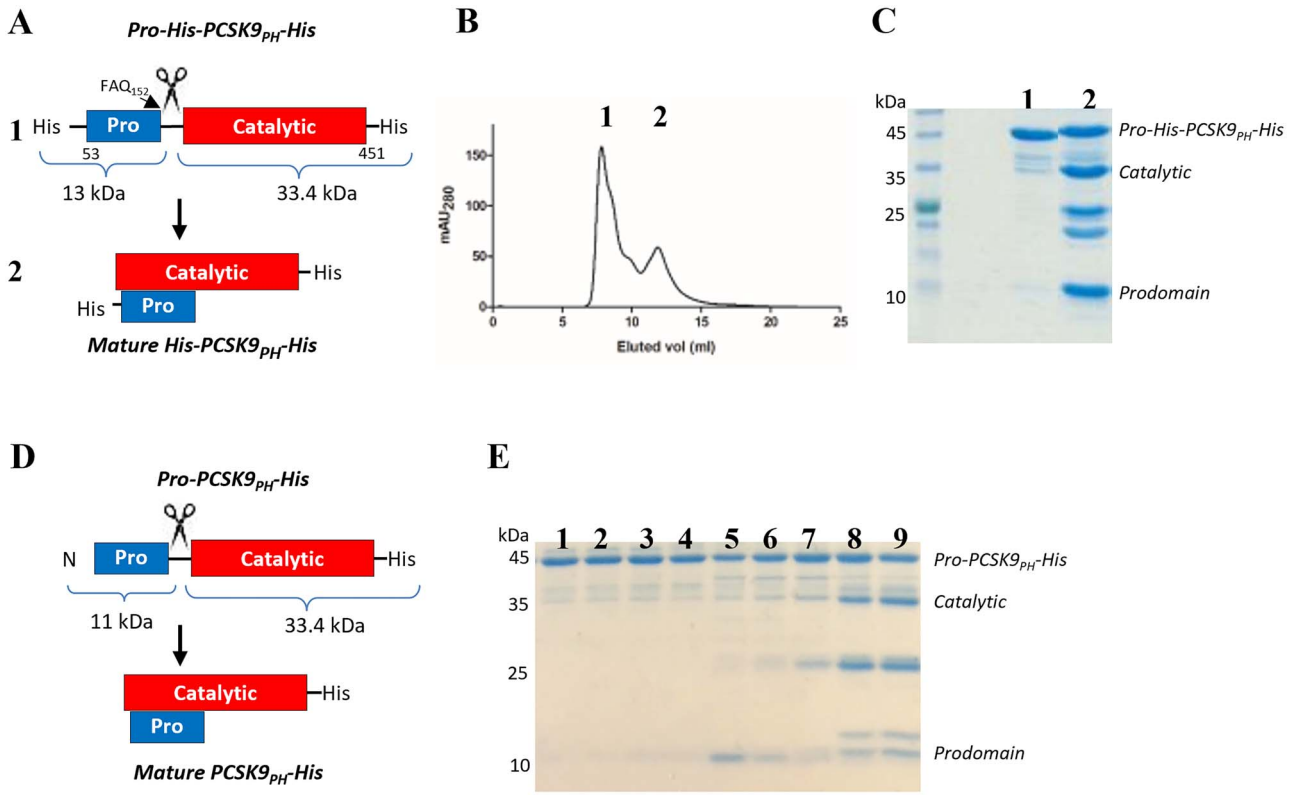

Fig. 1. Expression and purification of PCSK9PH in *E. coli*. (A) Schematic representation of the truncated PCSK9PH and its domains. Mature PCSK9PH was formed following autocleavage at the FAQ152↓SIP site between the prodomain and the catalytic domain. (B) His-PCSK9PH-His was purified by Ni-NTA affinity chromatography, followed by SEC. The SEC chromatogram of the eluted protein revealed two versions of PCSK9: (1) pro-PCSK9PH (not active) and (2) mature PCSK9PH (active). (C) Eluted fractions were concentrated and loaded onto a SDS-PAGE 12% gel. Lanes 1 and 2 represent the central peaks of the chromatogram: (1) a single band for uncleaved pro-His-PCSK9PH-His (46.4 kDa), and (2) multiple bands that include the proform (46.4 kDa) and the mature form, seen on the gel as a band for the catalytic domain (33.4 kDa) and a second band for the prodomain (13 kDa). (D) Schematic representation of PCSK9PH-His. (E) Nine SEC elution fractions of the purified PCSK9PH-His protein were loaded onto a SDS-PAGE gel. The last two fractions, in lanes 8 and 9, include the uncleaved pro-PCSK9PH-His (44.4 kDa), the catalytic domain (33.4 kDa) and the prodomain (11 kDa).

this domain is known to bind LDLR tightly in the acidic environment of the endosome, thereby assisting in promoting lysosomal degradation of the receptor. Importantly, deletion of the N-terminal residues 31–52 of the prodomain has been shown to result in a protein fragment that binds to LDLR at pH 7.4 with a >7-fold higher affinity than the full-length PCSK9 protein (Hyock *et al.* 2008), while not affecting the self-cleavage of PCSK9 (Du *et al.* 2011).

We started by producing a shorter version of PCSK9$_{PH}$ in *E.coli*, i.e. a version with residues 53–421, a sequence that is based on a published short version of the catalytic domain sequence (i.e. residues 153–421) (Alghamdi *et al.* 2015). However, the resulting purified protein was neither stable nor active, and it was degraded shortly after its purification (data not shown). In seeking a reason for this behavior, we noticed that in the PCSK9 structure (PDB ID 3P5B) the 422-DVINEAWFPEDQRVLTPNLVAALPPSTHGA-451 segment is largely hydrophobic (hydrophobic amino acids are underlined), and its residues turn toward the core of the catalytic domain (Fig. S1). Therefore, removing this segment probably affected the overall structure and function of the protein, thereby explaining the instability of the shorter PCSK9 fragment (i.e. residues 53–421) that we had produced. A review of the literature revealed that positions 422–451 are part of a hinge region connecting the catalytic domain to the C-terminal domain of PCSK9 (Saavedra *et al.* 2012) and that there is additional evidence that the C-terminal domain starts at position 452 and not before that (Horton *et al.* 2009; Lambert *et al.* 2009; Nishikido and Ray 2019), suggesting that the catalytic domain ends at position 451. Thus, we included the segment with residues 422–451 in the new truncated PCSK9$_{PH}$ proteins that we subsequently produced.

Two new truncated PCSK9$_{PH}$ proteins were thus expressed in the *E. coli* BL21 bacterial system, namely, a 46.4-kDa His-PCSK9(53-451)-His fragment (designated His-PCSK9$_{PH}$-His) and a 44.4-kDa PCSK9(53-451)-His fragment (designated PCSK9$_{PH}$-His), with yields of ~0.9 mg and ~0.5 mg protein/L of culture, respectively (Fig. 1). The design of His-PCSK9$_{PH}$-His derived from the noncovalent nature of the bond between the prodomain and the catalytic domain: since we wanted to retrieve both domains by Ni-NTA affinity chromatography, each domain was fused with a His-tag. The design of PCSK9$_{PH}$-His was based on our observation that a fragment with only one C-terminal His-tag could also be purified to yield both domains. However, its prodomain was less dominant, based on the band intensity (at 11 kDa) on the SDS-PAGE analysis.

The bacterial expression system produced both the proforms and the mature forms of His-PCSK9$_{PH}$-His and PCSK9$_{PH}$-His, indicating that the expressed proteins are largely stable to autocleavage (and self-activation) and that

only a small fraction of each expressed protein had been processed to become mature during protein purification (Fig. 1B, C and E). We note that the pro-PCSK9$_{PH}$ is a precursor form and is inactive, namely, unable to bind to LDLR, whereas the mature form is active, as is shown by two bands representing the prodomain and the catalytic domain (Fig. 1C and E). Both versions of the truncated PCSK9$_{PH}$, namely, His-PCSK9$_{PH}$-His and PCSK9$_{PH}$-His, were purified in the same way, and the resulting bands exhibited the same patterns on SEC. Since pro-PCSK9$_{PH}$ and mature PCSK9$_{PH}$ have the same sizes under native conditions, it is not surprising that they could not be separated by SEC, as can be seen in lane 2 of the gel (a single peak in Fig. 1B, but multiple bands in Fig. 1C).

His-PCSK9$_{PH}$-His protein identification by mass spectrometry

Purification of His-PCSK9$_{PH}$-His in the bacterial system resulted in additional two bands (at ∼25 and ∼20 kDa) that did not match the sizes of the prodomain, the catalytic domain or pro-PCSK9$_{PH}$, as can be seen in the gel of Fig. 1C. MS/MS was used to analyze and identify the unknown protein bands and the other dominant bands in lane 2 of Fig. 1C. The results showed a match between all these proteins and protein fragments to the human PCSK9 protein sequence (NCBI accession NP_777596.2), according to alignment between the peptides derived from each protein to the sequence of the WT PCSK9 protein. A summary of the matched identity for all peptides is presented in Table . These results confirm that all the bands in lane 2 of Fig. 1C represent proteins that are fragments of the recombinant truncated His-PCSK9$_{PH}$-His and not contaminants. It seemed reasonable to assume that this verification of the origin of the bands as deriving from the PCSK9 sequence would also hold for the recombinant truncated PCSK9$_{PH}$-His.

Truncated PCSK9$_{PH}$-His binds cell-expressed LDLR

Since His-PCSK9$_{PH}$-His and PCSK9$_{PH}$-His showed similar profiles in terms of product purity and since they basically comprised the same fragments in the same ratios, we chose to conduct the subsequent experiments with the least modified of the two forms, namely, PCSK9$_{PH}$-His (which has His only on its C-terminal). PCSK9$_{PH}$-His was subjected to flow-cytometric analysis to evaluate its ability to bind to native membrane-bound LDLR in HepG2 cells, which are known to express LDLR (Pak *et al.* 1996). The levels of LDLR expression in the cells were assessed by reaction with an anti-LDLR-PE antibody. The signal for LDLR expression at PCSK9$_{PH}$-His concentrations of 0.5 μM and 1 μM exhibited a low (14.5%), albeit dose-dependent, response in comparison to that for the control unstained HepG2 cells (Fig. S2A and B). To increase LDLR expression levels, the cells were treated either with the statin drug pravastatin or with LPDS. Pravastatin was used because it is known to upregulate cellular LDLR expression (Goto *et al.* 1997; Yu *et al.* 2017) as a side effect to its mode of action of blocking the pathway for cholesterol synthesis by inhibiting the intracellular enzyme, 3-hydroxy-3-methyl-glutaryl-coenzyme A (HMG-CoA) reductase (Istvan 2003). Pravastatin, 10 μM, was added to the culture medium of the HepG2 cells for 12 h, 24 h, or 48 h, or 4 days. The results showed a gradual increase in LDLR levels (Fig. S2C), with a maximal level of 63.6% after 4 days, in comparison to the control. As an alternative treatment, the FBS in the culture medium was replaced with 5% LPDS (giving a cholesterol-free medium), since it is known that the transcription of LDLR is activated in a regulatory feedback mechanism in the absence of extracellular cholesterol in the medium (Kawabe *et al.* 1999). The results showed a high level of LDLR expression at 24 h, reaching a maximum of 97.5% (Fig. S2D). Since the effect of LPDS on LDLR levels thus appeared to be superior to that of pravastatin, we continued to work with LPDS in the subsequent experiments. For analysis of the binding of PCSK9$_{PH}$-His to native membrane-bound LDLR, HepG2 cells were thus treated with LPDS for 24 h before being incubated with PCSK9$_{PH}$-His. A high binding level of 99.6% between PCSK9$_{PH}$-His and LDLR was detected (Fig. S2E), in agreement with the high levels of LDLR on the cell surface. Taken together, these results confirmed that the purified truncated PCSK9$_{PH}$-His recognizes and binds LDLR in a dose–response manner.

PCSK9$_{PH}$-His colocalizes with both intracellular and surface LDLR in HepG2 cells

To determine whether PCSK9$_{PH}$-His undergoes internalization into cells upon binding to LDLR, when added extracellularly, we performed live-cell confocal microscopy analysis. HepG2 cells were transfected with a pCDNA4-LDLR-EYFP construct that contains the *LDLR* gene fused to a C-terminal EYFP fluorescent protein. PCSK9$_{PH}$-His, labeled with the fluorescent dye Alexa Fluor 647 (1 μM), was incubated with the cells at room temperature for 10 min and 1.5 h, and the medium was then replaced with fresh medium. The colocalization of PCSK9$_{PH}$-His and LDLR was determined by confocal laser-scanning microscopy at 10 min and 1.5 h after adding PCSK9$_{PH}$-His.

The results showed that labeled PCSK9$_{PH}$-His (shown in red in Fig. S3A) accumulated on the cell surface shortly (10 min) after adding it to the cell medium and that there was strong colocalization of PCSK9$_{PH}$-His with LDLR (shown in green in Fig. S3A) on the surfaces of the two cells in the frame in Fig. S3A. Transiently expressed LDLR was visible both inside the cell and on the cell surface. After an additional 1.3 h, PCSK9$_{PH}$-His was seen inside the cell but less so on the cell surface. Colocalization of PCSK9$_{PH}$-His and LDLR was also observed inside the cell (Fig. S3B), in small circular structures, possibly representing endocytic vesicles (indicated by white arrows on the right panels). These findings suggest that truncated PCSK9$_{PH}$-His was internalized into the cells following interaction with LDLR. They also validate our premise that this shorter version of the PCSK9 protein functions (in terms of binding to LDLR and internalization to hepatic cells) similarly to the full-length wild-type PCSK9 protein.

Binding of PCSK9$_{PH}$ proteins to recombinant LDLR

SPR was used to evaluate the binding affinity between the PCSK9$_{PH}$ proteins and LDLR and the dependence of the binding on pH. The first step in these experiments was to test whether the His-tag had had any influence on binding (especially under acidic conditions). We therefore started the series of experiments with the protein having two His-tags, i.e. His-PCSK9$_{PH}$-His. The purified extracellular region (residues 22–788, ectodomain) of LDLR was covalently immobilized by amine coupling to a GLC sensor chip. For the mature

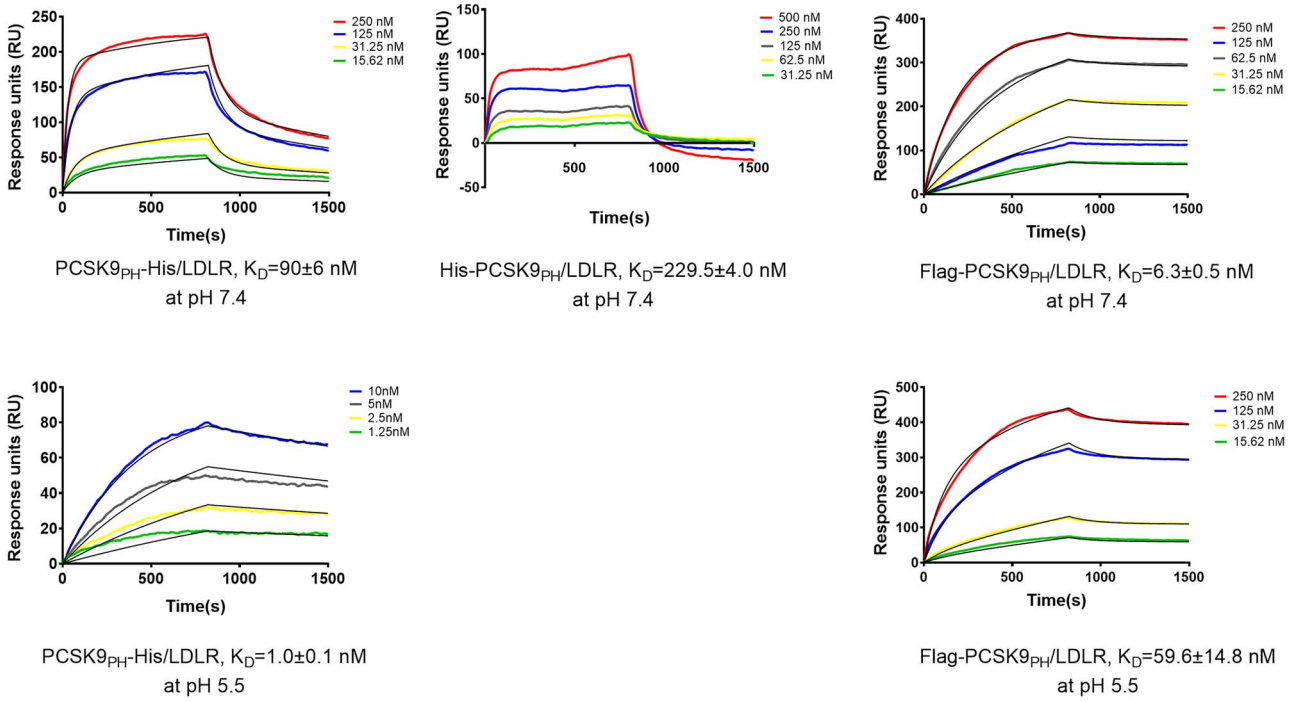

Fig. 2. SPR binding at pH 7.4 and pH 5.5. Representative SPR sensorgrams show the response over time (resonance units, RU) during the association and disassociation binding phases at pH 7.4 and pH 5.5 of purified soluble PCSK9 proteins to an immobilized recombinant LDLR ectodomain. (A) The affinity of PCSK9$_{PH}$-His for LDLR is enhanced at acidic pH by ∼90-fold relative to its affinity at pH 7.4 (KD = 90 nM). (B) At pH 7.4, His-PCSK9PH binds to LDLR with a low binding affinity of KD = 229.5 nM (but the binding affinity could not be measured in acidic pH, as His-PCSK9PH does not dissociate from LDLR at this pH). (C) The most potent, pH-selective protein, Flag-PCSK9PH, showed the highest binding affinity to LDLR at pH 7.4 (6.3 nM; 31.9 times stronger than WT PCSK9-His). Of note, the affinity of Flag-PCSK9PH for LDLR was reduced at acidic pH (KD = 59.6 nM) by ∼10-fold relative to its affinity at pH 7.4 (KD = 6.3 nM). For His-PCSK9PH-His, at both pH 7.4 and 5.5, the KD value was determined by steady-state analysis (see Fig. S5). For His-PCSK9PH-His (at pH 7.4) and Flag-PCSK9PH (at both pH 7.4 and 5.5) (fit shown as thin dark curves), a kinetic analysis of two-state binding model was used to determine the KD value. This assay was performed in triplicate.

His-PCSK9$_{PH}$-His, binding constants were obtained for a series of five concentrations, from 15.62 to 250 nM, at the physiological pH of 7.4 or 1.25 to 20 nM at the acidic pH of 5.5 (Fig. S4B). The inactive prodomain version (i.e. Pro-His-PCSK9$_{PH}$-His) that was purified from *E. coli* was used as a negative control (Fig. S4C), and a purified version of the WT full-length PCSK9-His (WT-PCSK9-His) was used as a positive control (Fig. S4A).

WT-PCSK9-His bound to LDLR with an affinity of K_D = 201.5 nM at pH 7.4 but with higher affinity (K_D = 4.3 nM) at pH 5.5 (Fig. S4A, top and bottom panels, respectively), as expected from previous reports (Lambert *et al.* 2012). The enhanced affinity at the acidic pH stems from the 14 histidine residues in the WT-PCSK9 C-terminal domain (not including the His-tag) becoming positively charged and hence binding with the negatively charged residues of the LDLR LBD (Holla *et al.* 2011a). Since His-PCSK9$_{PH}$-His lacks this C-terminal domain, we believed that it would be incapable of binding to LDLR with the same high binding affinity as WT PCSK9-His at acidic pH (thereby contributing to the stability of LDLR). Contrary to expectations, however, we found that at acidic pH, irreversible binding occurred for His-PCSK9$_{PH}$-His, since there was no dissociation of the complex [although, as expected, at pH 7.4 His-PCSK9$_{PH}$-His bound to LDLR with a higher affinity (K_D = 15.4 nM) than WT-PCSK9-His] (Fig. S4B). The inactive Pro-His-PCSK9$_{PH}$-His protein was used as a negative control and, also as expected, showed no binding to LDLR at either physiological or acidic pH (Fig. S4C).

Since it was not possible to obtain affinity constants for His-PCSK9$_{PH}$-His at acidic pH, we used the truncated PCSK9$_{PH}$-His protein that has only one His-tag at the N-terminus. Measurements of its binding affinity to LDLR showed a much higher affinity at the acidic pH (K_D = 1 nM) than at the physiological pH (K_D = 90 nM) (Fig. 2, Table I). Since we thought it likely that the higher affinity at the acidic pH derived from the six histidines in the C-terminal His-tag (fused to PCSK9$_{PH}$) becoming positively charged and therefore binding to the negatively charged residues on the LDLR LBD, we set out to further investigate this issue. To this end, we purified two new versions of PCSK9$_{PH}$ in a mammalian expression system: His-PCSK9$_{PH}$, which has the His-tag on the N-terminal (as distinguished from PCSK9$_{PH}$-His used in the above experiments, which has the His-tag on the C-terminal) and Flag-PCSK9$_{PH}$, in which we replaced the N-terminal His-tag with a Flag tag (to avoid interactions between His and LDLR at the acidic pH). The purified proteins were concentrated and loaded onto a SDS-PAGE gel stained with Coomassie Brilliant Blue to verify their size and purity (Fig. 3).

All PCSK9$_{PH}$ proteins, with either two His-tags (in both the C- and N-termini) or with one His-tag, in either the C- or N-terminus, showed different binding affinities to the recombinant LDLR ectodomain (summarized in Table I). We assumed that the His-tag was responsible for background binding in addition to the specific binding between the PCSK9 catalytic domain and LDLR EGF-A. Nevertheless, since the inactive Pro-His-PCSK9$_{PH}$-His could not bind to LDLR at pH 7.4 or pH 5.5, it is unlikely that the His-tag per se interacts

Table I. SPR binding results obtained at physiological and acidic pH values

Analyte	K_D (nM) at pH 7.4	K_D (nM) at pH 5.5
WT PCSK9-His	201.5 ± 19.5	4.3 ± 0.7*
Pro-His-PCSK9$_{PH}$-His	No binding	No binding
His-PCSK9$_{PH}$-His	15.7 + 1.11	ND
PCSK9$_{PH}$-His	90 ± 6	1.0 ± 0.1
His-PCSK9$_{PH}$	229.5 ± 4.0*	ND
Flag-PCSK9$_{PH}$	6.3 ± 0.5	59.6 ± 14.8

A recombinant purified LDLR ectodomain ligand was immobilized on the sensor chip, and the soluble analytes were allowed to flow over the ligand. For each analyte, the K_D was calculated for the analyte-ligand reaction. The mature PCSK9$_{PH}$ proteins with one or two His-tags bound to LDLR with different affinities at pH 7.4. At the acidic pH of 5.5, these proteins either did not dissociate or exhibited an enhanced affinity for LDLR, similar to that of WT PCSK9. *These values were determined according to a steady-state affinity model (Fig. S5); all other values were determined by a kinetic binding model, namely, a two-state binding model. ND, not determined (i.e. these proteins bound to LDLR but did not dissociate, and an affinity constant could thus not be calculated).

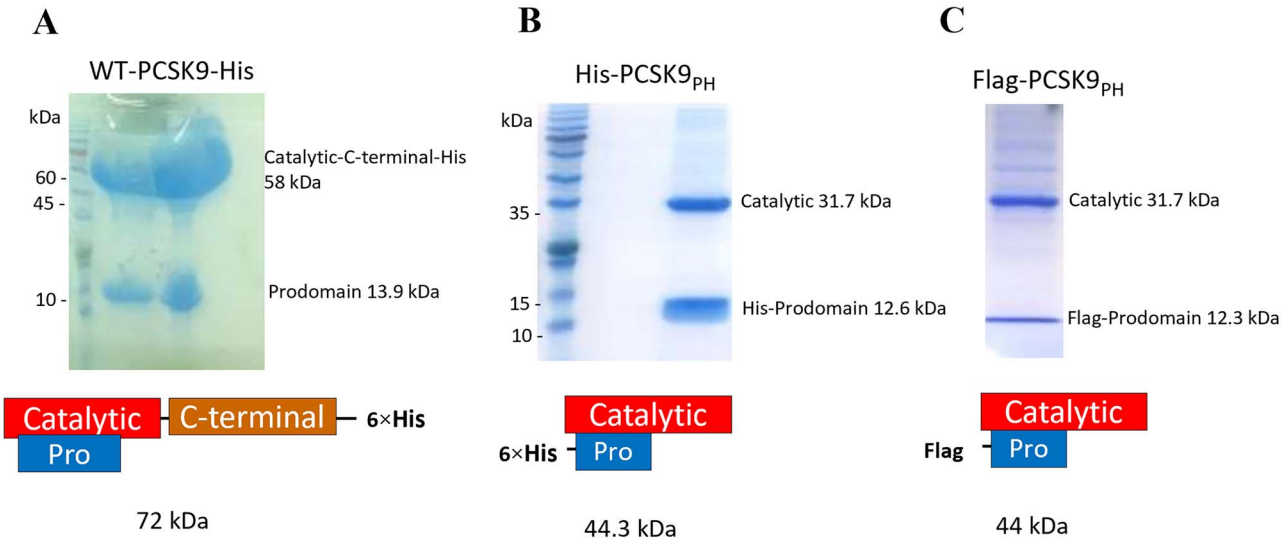

Fig. 3. Expression and purification of WT and PCSK9PH proteins in mammalian cells. WT-PCSK9 and PCSK9PH were expressed in FreeStyle™ 293-F cells and purified by affinity chromatography using either Ni-NTA or anti-FLAG beads. All proteins were of the expected size, seen as the two bands of the catalytic domain and the prodomain. (A) WT-PCSK9-His was expressed as a mature protein, seen on the gel as two bands (58 kDa and 13.9 kDa), with a yield of 14 mg/L of culture. (B) His-PCSK9PH also gave two bands of the mature form (31.7 kDa and 12.6 kDa), with a yield of 2 mg/L of culture. (C) The Flag-PCSK9PH mature form, seen on the gel as two bands (31.7 kDa and 12.6 kDa), was expressed with a lower yield (0.7 mg/L of culture) relative to WT-PCSK9-His and His-PCSK9PH.

with the receptor. Since the goal of this study was to engineer a PCSK9 protein with a high affinity for LDLR at pH 7.4 and a low affinity at an acidic pH, we replaced the His-tag with a Flag tag in PCSK9$_{PH}$. Indeed, at pH 7.4, the Flag-PCSK9$_{PH}$ showed higher binding affinity to LDLR (K_D = 6.3 nM) in comparison to WT PCSK9-His (K_D = ~201.5 nM), with a ~ 31.9-fold affinity enhancement (Fig. 2, Table I). Most importantly, at low pH, the affinity of Flag-PCSK9$_{PH}$ for LDLR decreased (K_D = ~59.6 nM), unlike the WT PCSK9-His, which exhibited enhanced binding to LDLR at low pH.

Flag-PCSK9$_{PH}$ inhibits the reduction of WT PCSK9-His-induced LDLR in HepG2 cells

To assess the effect of Flag-PCSK9$_{PH}$ on LDLR, we measured, by flow-cytometry analysis, the quantities of cell-surface LDLR in HepG2 cells treated with WT PCSK9-His, Flag-PCSK9$_{PH}$, or a combination of the two. To this end, HepG2 cells were cultured in the presence of LPDS to increase endogenous LDLR levels, and after 24 h the cells were incubated with the PCSK9 proteins for 12 h. As expected, treatment with 1 μM WT PCSK9-His decreased cell surface LDLR, whereas treatment with 1 μM Flag-PCSK9$_{PH}$ did not cause a decrease in cell-surface LDLR (Fig. 4), suggesting that Flag-PCSK9$_{PH}$ causes the cells to take up more exogenous LDL (vs. WT PCSK9-His). Of therapeutic importance, by treating the cells with a combination of WT PCSK9-His and Flag-PCSK9$_{PH}$, we were able to inhibit the effect of WT PCSK9-His on LDLR.

Flag-PCSK9$_{PH}$ increases LDL-C uptake in HepG2 cells

We next tested whether the ability of Flag-PCSK9$_{PH}$ to inhibit WT PCSK9-His-induced reduction of cell-surface LDLR levels could result in an enhancement in LDL-C uptake in HepG2 cells. For this purpose, flow-cytometry analysis was used to detect the level of fluorescently labeled LDL-C internalization into cells cultured with 5% LPDS and then treated with PBS, WT PCSK9-His (4 μM), Flag-PCSK9$_{PH}$ (4 μM), or a combination of WT PCSK9-His and Flag-PCSK9$_{PH}$ (4 μM). As shown in Fig. 5A, WT PCSK9-His decreased the uptake of LDL by 12.6%, whereas the Flag-PCSK9$_{PH}$ led to an increase of the LDL uptake by 29.7% versus the control. Treating the cells with a combination of WT PCSK9 and Flag-PCSK9$_{PH}$ also increased the uptake of LDL by 12.3%. Therefore, Flag-PCSK9$_{PH}$ was able to improve the ability of HepG2 to take up extracellular LDL-C. In addition, PBS-treated control HepG2

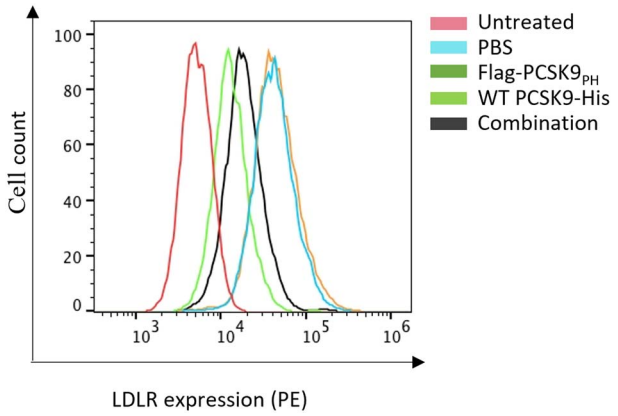

Fig. 4. Effects of PCSK9 proteins on the levels of cell-surface LDLR in HepG2 cells. The figure shows cell-surface LDLR levels as determined by flow cytometry. The experiment included untreated cells (pink, negative control) or cells treated with LPDS and PBS (light blue, positive control), WT PCSK9-His (green), Flag-PCSK9PH (orange) or a combination of WT PCSK9-His and Flag-PCSK9PH (black).

cells were visualized by an Operetta imaging system after incubation with LDL-Dylight 550 (Fig. 5B) with the aims to visually observe the uptake of LDL by the cells and to verify that the incubation time of 6 h with LDL-Dylight 550 was sufficient for detection. A close-up view of the cells confirms that 6 h were indeed sufficient for internalization of LDL-C into the cells.

Flag-PCSK9$_{PH}$ treatment leads to an accumulation of LDLR on the membrane but not in the lysosomes

Fluorescence imaging analysis with confocal microscopy confirmed the localization of WT PCSK9-His/LDLR complexes within the cell lysosomes (Fig. 6B, right panel, pink arrows), with overlapping coefficients values of 0.9, 0.8 and 0.8 for WT-PCSK9-His/lysosome, WT PCSK9-His/LDLR and LDLR/lysosome, respectively. More importantly, it showed that most lysosomes in Flag-PCSK9$_{PH}$-treated cells either contained Flag-PCSK9$_{PH}$ (Fig. 6A, left panel, red arrows) or were empty (Fig. 6A, right panel, green arrows) and did not contain LDLR, which was found mostly on the cell membrane (Fig. 6A, left panel, blue arrows). Here, overlapping coefficients values for Flag-PCSK9$_{PH}$/lysosome, Flag-PCSK9$_{PH}$/LDLR and LDLR/lysosome were 0.9, 0.4 and 0.3, respectively. These results indicate that whereas WT PCSK9-His treatment led to the accumulation of LDLR in the lysosomes for degradation (but not on the cell membrane), treatment with Flag-PCSK9$_{PH}$ led to the accumulation of membranal LDLR, which is ready to bind LDL-C for cell reuptake.

Discussion

We have shown that the pH-dependent disruption of the interaction of LDLR with PCSK9 could perhaps be exploited in the human body to lower plasma LDL-C and hence the risk of CVD—an idea investigated here at the cellular level, but one that warrants further investigation *in vivo*. Current concepts in drug development for hypercholesterolemia are focused on disrupting the functioning of PCSK9 by inhibiting its expression by small interfering RNA (siRNA) gene silencing or antisense oligonucleotides or by inhibiting the binding of PCSK9 to LDLR with monoclonal antibodies (mAbs) or peptides (Latimer *et al.* 2016; Seidah *et al.* 2019; Steffens *et al.* 2020). Nevertheless, to date, the only FDA-approved drugs are the mAbs evolocumab (Raal *et al.* 2015) and alirocumab (Schwartz *et al.* 2014), which target circulating PCSK9 by binding to its catalytic domain and blocking its interaction with LDLR. Clinical trials showed that in some patients these mAbs did indeed effectively lower blood cholesterol levels (Sabatine *et al.* 2017; Schwartz *et al.* 2018), but in others they were ineffective (Matta *et al.* 2020). A possible problem associated with these approaches for silencing PCSK9 expression or targeting it outside the hepatocyte derives from the fact that PCSK9 is also present in other organs and tissues, including the central nervous system, intestines, kidney, adipose tissues and macrophages (O'Connell and Lohoff 2020; Stoekenbroek *et al.* 2018). This raises the question of whether the inhibition of PCSK9 will also affect non-hepatic tissues, and, if so, how. Another problem in drug development for hypercholesterolemia is that PCSK9 targets LDLR for degradation by two routes—extracellular, in which PCSK9 exits the cell and binds LDLR on the cell surface, and intracellular, in which PCSK9 enters an endosome directly from the Golgi apparatus of the cell, binds LDLR, and then reroutes it to the lysosomes for degradation, thereby preventing the receptor from recycling (Holla *et al.* 2007; Lagace *et al.* 2006; Poirier *et al.* 2009). The development of mAbs has thus far focused on inhibiting PCSK9–LDLR binding by targeting extracellular PCSK9, with only limited attempts being made to target or modulate the intracellular PCSK9 pathway.

In this study, our goal was to develop an alternative approach for inhibiting PCSK9-mediated LDLR degradation as a means of enhancing LDLR recycling by the extracellular route and hence of reducing blood cholesterol levels. Our findings establish proof of principle for the utility of a pH-dependent truncated PCSK9 antagonist to control the PCSK9-LDLR interactions and thereby to regulate plasma cholesterol homeostasis for the treatment of hypercholesterolemia. While investigating this strategy, we also shed light on the structural implications and basic understanding of the pH-sensitive mechanism. In this mechanism, the truncated PCSK9 antagonist targets LDLR by binding to its EGF-A site, thereby interfering with LDLR–WT PCSK9 binding. We posit that this mode of action will not impair LDLR but rather promote its recycling and thereby enhance LDL-C uptake. With regard to the intracellular PCSK9-LDLR interactions, it still remains to be determined definitively whether our approach could antagonize the intracellular pathway of LDLR degradation, as will be the subject of a follow-up study.

Our approach to designing the truncated PCSK9-based antagonist (derived from the human WT PCSK9 protein) was based on two considerations. The first was the need to ensure the structural integrity, stability and activity of the truncated protein by retaining the prodomain and the catalytic domain (allowing self-cleavage and subsequent stable reassociation between the prodomain and the catalytic domain). The second was based on the mode of binding between PCSK9 and LDLR. The binding affinity of PCSK9 to LDLR changes as a function of pH: at the physiological pH of 7.4 (in the extracellular medium or in the cytosol) the binding of PCSK9 to LDLR is weak, but it becomes strong when PCSK9 binds LDLR at pH 5.5–6.0 upon entry into lysosomes (Yamamoto *et al.* 2011). With this in mind, our rational design for a PCSK9 antagonist was that it would bind LDLR strongly at pH 7.4 and weakly at pH 5.5–6.0.

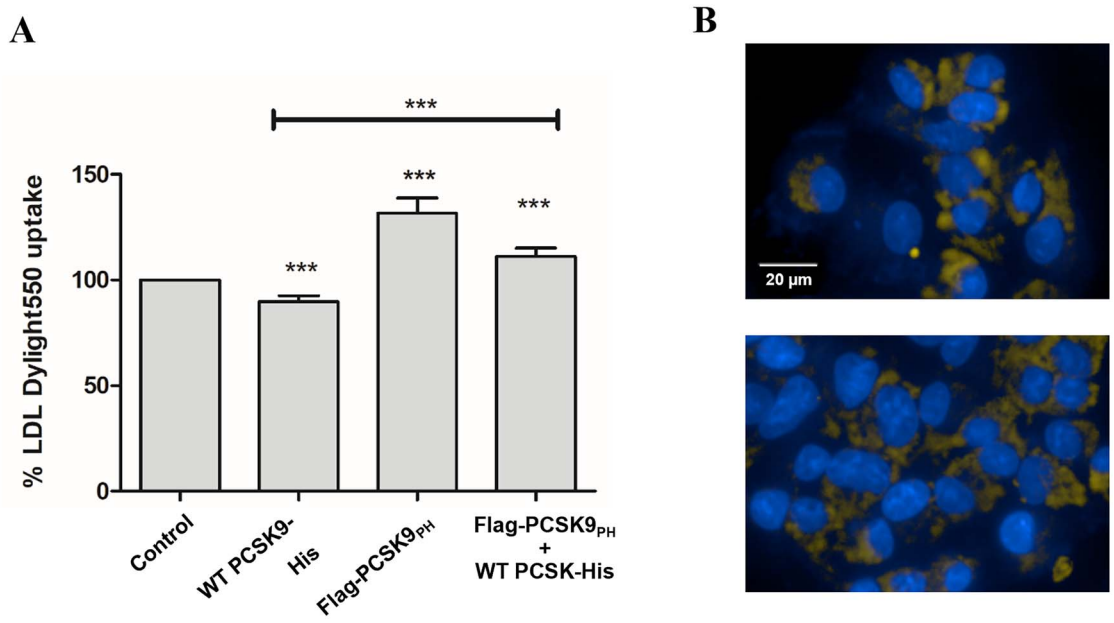

Fig. 5. Fluorescent LDL-C uptake assay after PCSK9 treatments. (A) HepG2 cells were treated with PBS, WT PCSK9-His (4 μM), Flag-PCSK9PH (4 μM) or both WT PCSK9-His and Flag-PCSK9$_{PH}$ (4 μM) for 12 h. Thereafter, LDL-Dylight 550 (20 μg/ml) was incubated with the cells for 6 h, and the fluorescent signal for LDL-C was analyzed in a flow cytometer. Data are presented as mean percentages ± SD for three independent experiments performed in duplicate. Statistical analysis was performed using Student's t-test, $^{***}P < 0.0001$. (B) HepG2 control cells (PBS treatment) were imaged using an Operetta imaging system after 6 h of incubation with LDL-Dylight 550. Two fields from one well are shown, with a scale bar of 20 μm. Cell nuclei stained with Hoechst 33342 (blue) and LDL-C (yellow droplets) are visible inside the cells.

We thus started by producing the shortest version of a truncated PCSK9 that was both stable and active, namely, one that contains the PCSK9 prodomain and catalytic domain (designated PCSK9$_{PH}$). The PCSK9 C-terminal domain that is responsible for the strong PCSK9-LDLR interaction at lysosomal pH of 5.5–6.0 (Yamamoto *et al.* 2011) and for mediating LDLR degradation was removed, thereby abrogating the ability of the truncated PCSK9 to direct/lead LDLR to degradation (Marsh *et al.* 2018; Saavedra *et al.* 2012). In addition, the N-terminal acidic residues of the prodomain were removed to increase its affinity for LDLR at physiological pH (Holla *et al.* 2011b).

Our data indicate that deletion of the above two segments, i.e. residues 31–52 of the prodomain and residues 452–692 of the C-terminal domain, resulted in a ∼32-fold higher affinity of Flag-PCSK9$_{PH}$ (vs. WT PCSK9-His) for LDLR, which confirmed our notion that the truncated PCSK9 (i.e. Flag-PCSK9$_{PH}$) can indeed compete with WT PCSK9-His for binding to LDLR at pH 7.4. This finding provides support for our working hypothesis that an antagonist (truncated PCSK9 in this case) that binds to LDLR with higher affinity than the WT at the physiological pH but with low affinity at the acidic pH of the early endosome and the endosome will interfere with LDLR–WT PCSK9 binding, thereby allowing LDLR to dissociate from the complex and 'escape' the degradation path in the lysosomes. Further support for this notion may be found in a number of studies: Holla *et al.* clearly showed enhanced PCSK9 pH-dependent binding to both full-length LDLR and LDLR lacking the LBD (Holla *et al.* 2011a). Similarly, Yamamoto *et al.* show dramatically increased binding at an acidic pH by a PCSK9 lacking the C-terminal domain (Yamamoto *et al.* 2011). These results could not have been obtained if the only determinant of pH-dependent binding was the binding of the C-terminus of PCSK9 to the LBD of LDLR. Evidence from crystal structures suggests that H306 in the LDLR EGFA domain is also a component of the pH effect (McNutt *et al.* 2009). These three studies suggest that although the mechanism of PCSK9-induced internalization of LDLR is not completely understood, an important component of the mechanism is the increased interaction of the C-terminus domain of PCSK9 with the LBD of LDLR.

Our results showed that Flag-PCSK9$_{PH}$ significantly enhanced (by 29.7%) internalization/uptake into the cells of LDL-C from the extracellular environment. In contrast, WT PCSK9-His decreased the LDL-C uptake (by 12.6%), as was expected, since the Cys/His-rich C-terminal domain of WT PCSK9 is known to bind tightly to the LBD of LDLR, thereby reducing LDLR levels on the cell surface. Since Flag-PCSK9$_{PH}$ does not contain this C-terminal domain, it was predicted that Flag-PCSK9$_{PH}$ would not bind tightly to LDLR in the acidic environment of the endosome and would therefore easily dissociate from the Flag-PCSK9$_{PH}$–LDLR complex, enabling the LDLR to recycle to the cell surface to take up more LDL-C. The strong induction of LDL-C uptake by the addition of Flag-PCSK9$_{PH}$ (29.7%) in comparison with the inhibitory effect of WT PCSK9-His (12.6%) may be due to the presence of endogenous PCSK9 (extracellular and/or intracellular) (Holla *et al.* 2007; Lagace *et al.* 2006; Poirier *et al.* 2009). However, the levels and activity of endogenous PCSK9 may not necessarily be constant, since the levels may be raised due to LDLR overexpression (Attie and Seidah 2005) or the activity may be enhanced due to post-translational modifications (e.g. glycosilation) and/or endogenous PCSK9 may be less susceptible to cleavage by proteases (e.g. furin) (Benjannet *et al.* 2006), all of which would result in low (almost minimal) basal levels of LDL-C uptake. Our results also showed that treating HepG2 cells with a combination of Flag-PCSK9$_{PH}$ and WT PCSK9-His

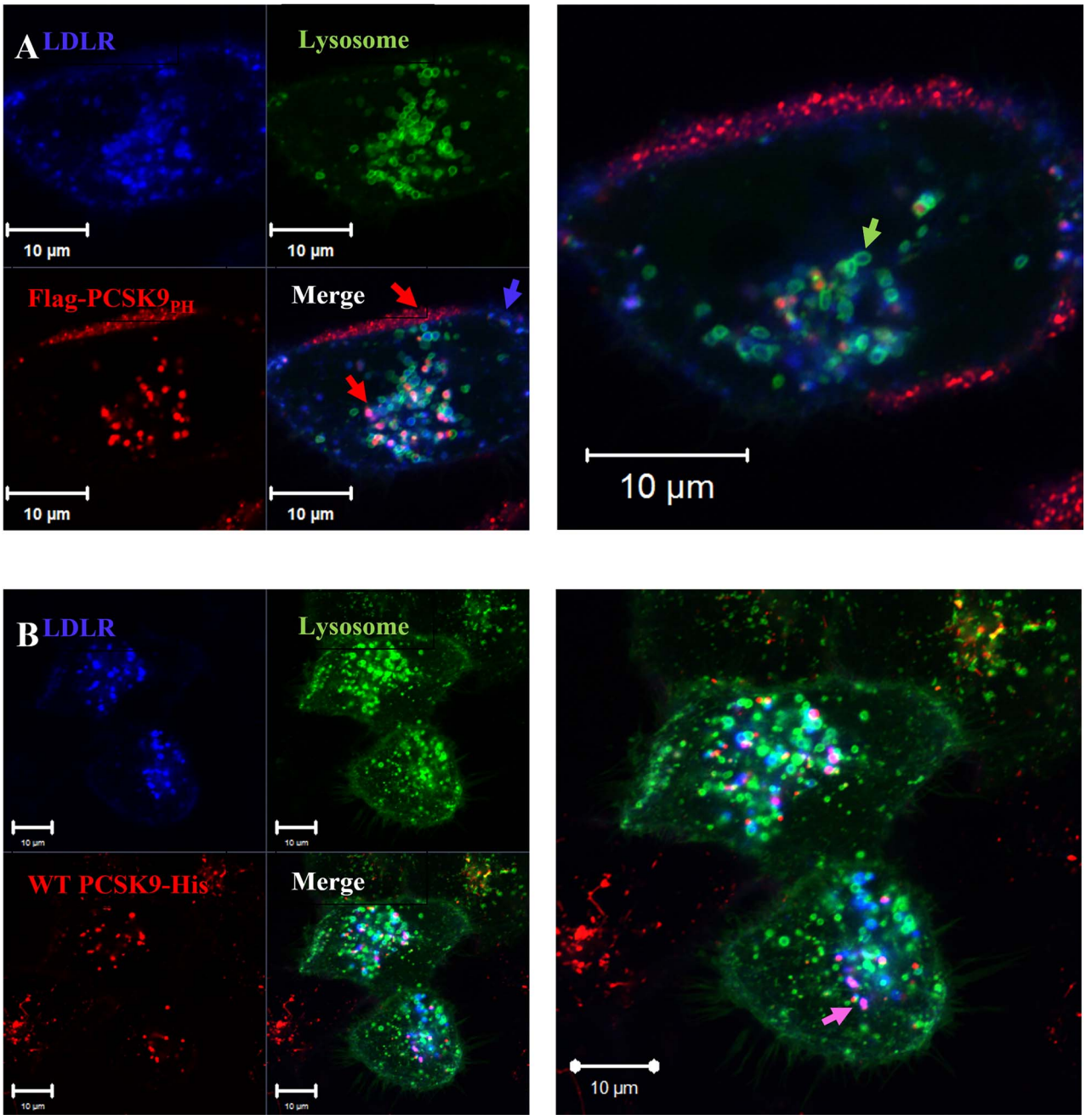

Fig. 6. ocalization of PCSK9 proteins, LDLR and lysosomes within HepG2 cells. (A) Live imaging showing either Flag-PCSK9$_{PH}$ positive/LDLR negative (left, red arrows) or empty (right, green arrows) lysosomes in cells treated with Flag-PCSK9$_{PH}$. These images also show membranal LDLR (left, blue arrows). (B) Localization of WT PCSK9-His/LDLR complexes within lysosomes (right, pink arrows). In this experiment, the PCSK9 proteins were labeled with Alexa Fluor 647 (red), LDLR with BFP (blue) and the lysosomes with GFP (green). Scale bar, 10 μm.

similarly demonstrated the improved ability—by 12.3%—of the hepatic cells to take up extracellular LDL. This finding confirms that truncated Flag-PCSK9$_{PH}$ can indeed compete with WT PCSK9-His for binding to LDLR on the cell surface. In the LDL uptake experiment, WT PCSK9-His was exposed to different concentrations of Flag-PCSK9$_{PH}$, ranging from 500 nM to 4 μM. At 2, 3 and 4 μM Flag-PCSK9$_{PH}$, there was a significant uptake of LDL, and it is therefore possible that at higher levels of Flag-PCSK9$_{PH}$, this effect of Flag-PCSK9$_{PH}$ on LDL uptake would increase even further.

Of note, the high concentration of PCSK9 proteins (4 μM) used in our cellular assays could also have caused a nonspecific effect, perhaps by interaction of the PCSK9 protein with the LDL particle or the cell surface. For instance, PCSK9 is known to bind not only to LDL particles but also to cell-surface heparan sulfate proteoglycans (HSPGs). It has been shown that binding to cell-surface HSPGs enhances PCSK9 binding to LDLR and hence to LDLR degradation in HepG2 cells (Gustafsen *et al.* 2017). Therefore, it seems reasonable to conclude that an inhibitory effect could also be enhanced as a result of a cooperative binding of PCSK9 to HSPG.

In conclusion, our strategy for WT PCSK9 inhibition with the truncated PCSK9 antagonist, Flag-PCSK9$_{PH}$, may have several advantages over current approaches that directly target WT PCSK9. These include: (i) Flag-PCSK9$_{PH}$ is derived from human WT PCSK9, and therefore there is a good probability that it will be nonimmunogenic. (ii) Flag-PCSK9$_{PH}$ binds to the EGF-A site of LDLR, and it will compete with the WT PCSK9 for binding to LDLR, but it will not impair the LDLR function of taking up LDL-C because LDL-C binds to the LBD (not EGF-A) on LDLR. (iii) In the acidic environment of the endosome, Flag-PCSK9$_{PH}$ has the potential to dissociate from the Flag-PCSK9$_{PH}$–LDLR complex and will thus not direct LDLR to the lysosome for degradation. This is because Flag-PCSK9$_{PH}$ lacks the original C-terminal domain that is used by WT PCSK9 to 'lock' LDLR into an open conformation and hence to prevent it from escaping the degradation pathway (Saavedra *et al.* 2012). (iv) Flag-PCSK9$_{PH}$ may inhibit both the intra- and extracellular routes of WT PCSK9-mediated LDLR degradation, as it has the potential to remain bound to LDLR after internalization in the early endosome and thus block the access of WT PCSK9 to the binding site on LDLR. (v) Flag-PCSK9$_{PH}$ does not interact with WT PCSK9 and therefore does not impair its functioning in other physiological roles.

We believe that we are on track to developing a new approach to counteracting hypercholesterolemia. Our future work will focus on validating our hypothesis that Flag-PCSK9$_{PH}$ does not direct LDLR to degradation and that the receptor dissociates from Flag-PCSK9$_{PH}$ at the endosome phase. We plan to do so by tracking the movement of Flag-PCSK9$_{PH}$ and LDLR from initial binding on the cell surface to the lysosome by using live imaging. Evidence that Flag-PCSK9$_{PH}$ and LDLR dissociate in the early endosome and do not continue to the lysosome will validate the notion that Flag-PCSK9$_{PH}$ remains bound to LDLR until it dissociates, which means it may also compete with and prevent WT PCSK9 from binding to LDLR in the endosome in the intracellular route.

As discussed above, there are some problems associated with the efficacy of PCSK9 inhibitors as therapeutics for hypercholesterolemia: in some cases mAbs are ineffective when used alone to reduce the LDL-C levels (Schmidt *et al.* 2017), and statins actually induce PCSK9 (Zhao *et al.* 2019), which makes them ineffective in reducing plasma LDL-C (Dubuc *et al.* 2004; Schulz *et al.* 2015). Therefore, it would seem that an alternative strategy, such as the one proposed here, to directly target and neutralize PCSK9 should be sought.

Authors' contributions

L.B., I.K. and N.P. designed the research; L.B. performed the research; L.B., I.K. and N.P. analyzed the data; L.B. and N.P. wrote the paper.

Supplementary data

Supplementary data are available at *PEDS* online.

Acknowledgments

The authors thank May Meltzer, Dr Alon Zilka and Dr Uzi Hadad for their technical assistance. FACS experiments were performed at the Ilse Katz Institute for Nanoscale Science and Technology, BGU. Confocal microscopy experiments were performed at the NIBN proteomics unit, BGU.

Funding

The Israel Science Foundation [grant number 615/14 to N.P.].

Conflict of Interest

The authors declare that they have no conflict of interest with respect to publication of this paper.

References

Alghamdi, R.H., O'Reilly, P., Lu, C., Gomes, J., Lagace, T.A. and Basak, A. (2015) *Eur. J. Med. Chem.*, **92**, 890–907.
Attie, A.D. and Seidah, N.G. (2005) *Cell Metab.*, **1**, 290–292.
Awan, Z., Baass, A. and Genest, J. (2014) *Clin. Chem.*, **60**, 1380–1389.
Beglova, N. and Blacklow, S.C. (2005) *Trends Biochem. Sci.*, **30**, 309–317.
Beglova, N., Jeon, H., Fisher, C. and Blacklow, S.C. (2004) *Mol. Cell*, **16**, 281–292.
Benjannet, S., Rhainds, D., Essalmani, R. *et al.* (2004) *J. Biol. Chem.*, **279**, 48865–48875.
Benjannet, S., Rhainds, D., Hamelin, J., Nassoury, N. and Seidah, N.G. (2006) *J. Biol. Chem.*, **281**, 30561–30572.
Blacklow, S.C. (2007) *Curr. Opin. Struct. Biol.*, **17**, 419–426.
Brown, M.S., Herz, J. and Goldstein, J.L. (1997) *Nature*, **388**, 629–630.
Bui, Q.T., Prempeh, M. and Wilensky, R.L. (2009) *Int. J. Biochem. Cell Biol.*, **41**, 2109–2113.
Cannon, C.P., Blazing, M.A., Giugliano, R.P. *et al.* (2015) *N. Engl. J. Med.*, **372**, 2387–2397.
Cleeman, J.I. (2001) *JAMA*, **285**, 2486–2497.
Costet, P., Krempf, M. and Cariou, B. (2008) *Trends Biochem. Sci.*, **33**, 426–434.
Du, F., Hui, Y., Zhang, M., Linton, M.F., Fazio, S. and Fan, D. (2011) *J. Biol. Chem.*, **286**, 43054–43061.
Dubuc, G., Chamberland, A., Wassef, H., Davignon, J., Seidah, N.G., Bernier, L. and Prat, A. (2004) *Arterioscler. Thromb. Vasc. Biol.*, **24**, 1454–1459.
Edelheit, O., Hanukoglu, A. and Hanukoglu, I. (2009) *BMC Biotechnol.*, **9**, 61.
Fernández-Higuero, J.A., Benito-Vicente, A., Etxebarria, A., Milicua, J.C.G., Ostolaza, H., Arrondo, J.L.R. and Martín, C. (2016) *Sci. Rep.*, **6**, 36324.
Fisher, T.S., Surdo, P.L., Pandit, S. *et al.* (2007) *J. Biol. Chem.*, **282**, 20502–20512.
Gencer, B., Lambert, G. and Mach, F. (2015) *Swiss Med. Wkly.*, **145**.
Go, G.W. and Mani, A. (2012) *Yale J. Biol. Med.*, **85**, 19–28.
Goto, D., Okimoto, T., Ono, M., Shimotsu, H., Abe, K., Tsujita, Y. and Kuwano, M. (1997) *Arterioscler. Thromb. Vasc. Biol.*, **17**, 2707–2712.
Gustafsen, C., Olsen, D., Vilstrup, J. *et al.* (2017) *Nat. Commun.*, **8**, 503.
Hampton, E.N., Knuth, M.W., Li, J., Harris, J.L., Lesley, S.A. and Spraggon, G. (2007) *Proc. Natl. Acad. Sci. U.S.A.*, **104**, 14604–14609.
Hansson, G.K. and Hermansson, A. (2011) *Nat. Immunol.*, **12**, 204–212.
Hevonoja, T., Pentikäinen, M.O., Hyvönen, M.T., Kovanen, P.T. and Ala-Korpela, M. (2000) *Biochim. Biophys. Acta-Mol. Cell Biol. Lipids*, **1488**, 189–210.
Holla, Ø.L., Cameron, J., Berge, K.E., Ranheim, T. and Leren, T.P. (2007) *BMC Cell Biol.*, **8**, 9.
Holla, Ø.L., Cameron, J., Tveten, K., Strøm, T.B., Berge, K.E., Laerdahl, J.K. and Leren, T.P. (2011a) *J. Lipid Res.*, **52**, 1787–1794.
Holla, Ø.L., Laerdahl, J.K., Strøm, T.B., Tveten, K., Cameron, J., Berge, K.E. and Leren, T.P. (2011b) *Biochem. Biophys. Res. Commun.*, **406**, 234–238.

Horton, J.D., Cohen, J.C. and Hobbs, H.H. (2007) *Trends Biochem. Sci.*, **32**, 71–77.
Horton, J.D., Cohen, J.C. and Hobbs, H.H. (2009) *J. Lipid Res.*, **50**, S172–S177.
Hyock, J.K., Lagace, T.A., McNutt, M.C., Horton, J.D. and Deisenhofer, J. (2008) *Proc. Natl. Acad. Sci. U.S.A.*, **105**, 1820–1825.
Istvan E. (2003) Statin inhibition of HMG-CoA reductase: a 3-dimensional view. *Atheroscler Suppl.* **4**, 3–8.
Jeon, H. and Blacklow, S.C. (2005) *Annu. Rev. Biochem.*, **74**, 535–562.
Kawabe, Y., Suzuki, T., Hayashi, M., Hamakubo, T., Sato, R. and Kodama, T. (1999) *Biochim. Biophys. Acta-Mol. Cell Biol. Lipids*, **1436**, 307–318.
Lagace, T.A., Curtis, D.E., Garuti, R. *et al.* (2006) *J. Clin. Invest.*, **116**, 2995–3005.
Lakadamyali, M., Rust, M.J. and Zhuang, X. (2006) *Cell*, **124**, 997–1009.
Lambert, G., Charlton, F., Rye, K.A. and Piper, D.E. (2009) *Atherosclerosis*, **203**, 1–7.
Lambert, G., Sjouke, B., Choque, B., Kastelein, J.J.P. and Hovingh, G.K. (2012) *J. Lipid Res.*, **53**, 2515–2524.
Latimer, J., Batty, J.A., Neely, R.D.G. and Kunadian, V. (2016) *J. Thromb. Thrombolysis*, **42**, 405–419.
Libby, P. (2002) *Nature*, **420**, 868–874.
Lodish, H., Berk, A. and Zipursky, S. (2000) 4th edn. W. H. Freeman, W.H. Freeman & Co (Sd).
Luo, J., Jiang, L., Yang, H. and Song, B.L. (2017) *Traffic*, **18**, 209–217.
Mancini, G.B.J., Baker, S., Bergeron, J. *et al.* (2011) *Can. J. Cardiol.*, **27**, 635–662.
Marsh, W., Witten, A. and Stabenfeldt, S.E. Exploiting Phage Display for Development of Novel Cellular Targeting Strategies. *Methods Mol Biol.* 2018;**1831**:71–94.
Martínez-Oliván, J., Arias-Moreno, X., Hurtado-Guerrero, R., Carrodeguas, J.A., Miguel-Romero, L., Marina, A., Bruscolini, P. and Sancho, J. (2015) *FEBS Lett.*, **589**, 3534–3540.
Matta, A., Taraszkiewicz, D., Bongard, V. and Ferrières, J. (2020) *Am. J. Case Rep.*, **21**, 1–4.
McMahon, H.T. and Boucrot, E. (2011) *Nat. Rev. Mol. Cell Biol.*, **12**, 517–533.
McNutt, M.C., Kwon, H.J., Chen, C., Chen, J.R., Horton, J.D. and Lagace, T.A. (2009) *J. Biol. Chem.*, **284**, 10561–10570.
McNutt, M.C., Lagace, T.A. and Horton, J.D. (2007) *J. Biol. Chem.*, **282**, 20799–20803.
Moore, K.J., Sheedy, F.J. and Fisher, E.A. (2013) *Nat. Rev. Immunol.*, **13**, 709–721.
Nishikido, T. and Ray, K.K. (2019) *Front. Cardiovasc. Med.*, **5**, 199.
O'Connell, E.M. and Lohoff, F.W. (2020) *Front. Neurosci.*, **14**, 609.
Pak, Y.K., Kanuck, M.P., Berrios, D., Briggs, M.R., Cooper, A.D. and Ellsworth, J.L. (1996) *J. Lipid Res.*, **37**, 985–998.
Piper, D.E., Jackson, S., Liu, Q., Romanow, W.G., Shetterly, S., Thibault, S.T., Shan, B. and Walker, N.P.C. (2007) *Structure*, **15**, 545–552.
Poirier, S., Mayer, G., Poupon, V. *et al.* (2009) *J. Biol. Chem.*, **284**, 28856–28864.
Raal, F.J., Honarpour, N., Blom, D.J., Hovingh, G.K., Xu, F., Scott, R., Wasserman, S.M. and Stein, E.A. (2015) *Lancet*, **385**, 341–350.
Reiner, Z. (2014) *Nutr. Metab. Cardiovasc. Dis.*, **24**, 1057–1066.
Roth, Z., Weil, S., Aflalo, E.D., Manor, R., Sagi, A. and Khalaila, I. (2013) *Chem Bio Chem*, **14**, 1116–1122.
Rudenko, G., Henry, L., Henderson, K., Ichtchenko, K., Brown, M.S., Goldstein, J.L. and Deisenhofer, J. (2002) *Science (80-.)*, **298**, 2353–2358.
Saavedra, Y.G.L., Day, R. and Seidah, N.G. (2012) *J. Biol. Chem.*, **287**, 43492–43501.
Sabatine, M.S., Giugliano, R.P., Keech, A.C. *et al.* (2017) *N. Engl. J. Med.*, **376**, 1713–1722.
Salowe, S.P., Zhang, L., Zokian, H.J., Gesell, J.J., Zink, D.L., Wiltsie, J., Ai, X., Kavana, M. and Pinto, S. (2016) *J. Biomol. Screen.*.
Schmidt, A.F., Pearce, L.S., Wilkins, J.T., Overington, J.P., Hingorani, A.D. and Casas, J.P. (2017) *Cochrane Database Syst. Rev.*, **2017**, CD011748.
Schulz, R., Schlüter, K.D. and Laufs, U. (2015) *Basic Res. Cardiol.*, **110**, 4.
Schulze, H., Kolter, T. and Sandhoff, K. (2009) *Biochim. Biophys. Acta-Mol. Cell Res.*, **1793**, 674–683.
Schwartz, G.G., Bessac, L., Berdan, L.G. *et al.* (2014) *Am. Heart J.*, **168**, 682–689.e1.
Schwartz, G.G., Steg, P.G., Szarek, M. *et al.* (2018) *N. Engl. J. Med.*, **379**, 2097–2107.
Segrest, J.P., Jones, M.K., De Loof, H. and Dashti, N. (2001) *J. Lipid Res.*, **42**, 1346–1367.
Seidah, N.G., Prat, A., Pirillo, A., Catapano, A.L. and Norata, G.D. (2019) *Cardiovasc. Res.*, **115**, 510–518.
Sirtori, C.R. (2014) *Pharmacol. Res.*, **88**, 3–11.
Slater, H.R., McKinney, L., Packard, C.J. and Shepherd, J. (1984) *Arteriosclerosis*, **4**, 604–613.
Stancu, C. and Sima, A. (2001) *J. Cell. Mol. Med.*, **5**, 378–387.
Steffens, D., Bramlage, P., Scheeff, C., Kasner, M., Hassanein, A., Friebel, J. and Rauch-Kröhnert, U. (2020) *Expert Opin. Biol. Ther.*, **20**, 35–47.
Stoekenbroek, R.M., Lambert, G., Cariou, B. and Hovingh, G.K. (2018) *Nat. Rev. Endocrinol.*, **15**, 52–62.
Stolk, M.F.J., Becx, M.C.J.M., Kuypers, K.C. and Seldenrijk, C.A. (2006) *Clin. Gastroenterol. Hepatol.*, **4**, 908–911.
Surdo, P.L., Bottomley, M.J., Calzetta, A. *et al.* (2011) *EMBO Rep.*, **12**, 1300–1305.
Tveten, K., Holla, Ø.L., Cameron, J., Strøm, T.B., Berge, K.E., Laerdahl, J.K. and Leren, T.P. (2012) *Hum. Mol. Genet.*, **21**, 1402–1409.
Virani, S.S., Alonso, A., Benjamin, E.J. *et al.* (2020) *Circulation*, **141**, E139–E596.
Wierød, L., Cameron, J., Strøm, T.B. and Leren, T.P. (2016) *Mol. Genet. Metab. Reports*, **9**, 86–93.
Xpr, P., Interaction, P., System, A., Bronner, V., Bravman, T., Nimri, S. and Lavie, K. (2005) *Cytokine*. **3**, 11–18.
Xu, H. and Ren, D. (2015) *Annu. Rev. Physiol.*, **77**, 57–80.
Yamamoto, T., Lu, C. and Ryan, R.O. (2011) *J. Biol. Chem.*, **286**, 5464–5470.
Yu, Q., Chen, Y. and Xu, C.B. (2017) *Front. Pharmacol.*, **8**.
Zhang, D.W., Garuti, R., Tang, W.J., Cohen, J.C. and Hobbs, H.H. (2008) *Proc. Natl. Acad. Sci. U.S.A.*, **105**, 13045–13050.
Zhang, D.W., Lagace, T.A., Garuti, R., Zhao, Z., McDonald, M., Horton, J.D., Cohen, J.C. and Hobbs, H.H. (2007) *J. Biol. Chem.*, **282**, 18602–18612.
Zhao, Z., Du, S., Shen, S., Luo, P., Ding, S., Wang, G., Wang, L. and Omboni, S. (2019) Comparative efficacy and safety of lipid-lowering agents in patients with hypercholesterolemia: A frequentist network meta-analysis. *Med. (Baltimore)*, **98**, e14400.